Thermal Stability of Colloidal InP Nanocrystals: Small Inorganic Ligands Boost High-Temperature Photoluminescence

ARTICLE *in* ACS NANO · DECEMBER 2013

Impact Factor: 12.88 · DOI: 10.1021/nn405811p · Source: PubMed

Thermal Stability of Colloidal InP Nanocrystals: Small Inorganic Ligands Boost High-Temperature Photoluminescence

Clare E. Rowland,[†] Wenyong Liu,[‡] Daniel C. Hannah,[†] Maria K. Y. Chan,[§] Dmitri V. Talapin,[‡,§] and Richard D. Schaller[†,§,*]

[†]Department of Chemistry, Northwestern University, Evanston, Illinois 60208, United States, [‡]Department of Chemistry and James Frank Institute, University of Chicago, Chicago, Illinois 60637, United States, and [§]Center for Nanoscale Materials, Argonne National Laboratory, Argonne, Illinois 60439, United States

ABSTRACT We examine the stability of excitons in quantum-confined InP nanocrystals as a function of temperature elevation up to 800 K. Through the use of static and time-resolved spectroscopy, we find that small inorganic capping ligands substantially improve the temperature dependent photoluminescence quantum yield relative to native organic ligands and perform similarly to a wide band gap inorganic shell. For this composition, we identify the primary exciton loss mechanism as electron trapping through a combination of transient absorption and transient photoluminescence measurements. Density functional theory indicates little impact of studied inorganic ligands on InP core states, suggesting that reduced thermal degradation relative to organic ligands yields improved stability; this is further supported by a lack of size dependence in photoluminescence quenching, pointing to the dominance of surface processes, and by relative thermal stabilities of the surface passivating media. Thus, small inorganic ligands, which benefit device applications due to improved carrier access, also improve the electronic integrity of the material during elevated temperature operation and subsequent to high temperature material processing.

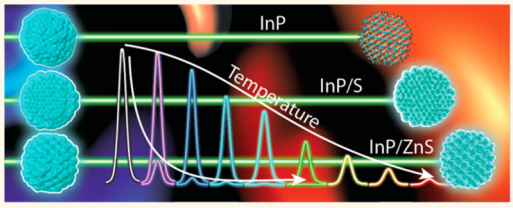

KEYWORDS: colloidal nanomaterials · thermal stability · inorganic ligands · transient absorption · static · time-resolved photoluminescence · PL quenching · semiconductors · InP

Interest in semiconductor nanocrystals (NCs) arises from promise regarding their practical application in areas as diverse as light-emitting diodes (LEDs),[1−3] lasers,[4,5] concentrated solar cells,[6,7] biolabels,[8] electronics,[9] and sensors.[10,11] However, surface passivation methods that maximize photoluminescence (PL) efficiency in some instances also impede utility in these very applications. For example, long-chain aliphatic capping ligands are commonly bound to a NC core, yet their presence creates an insulating barrier that encompasses the particle, effectively impeding the injection and extraction of electrons and holes. The addition of a wide band-gap type-I shell (*e.g.*, ZnS) to the NC is often a more effective means of surface passivation (*i.e.*, results in higher PL quantum yields), yet it also often contributes a significant barrier to electronic contact with the core. Thus, in both traditional core and core/shell NCs, surface passivation is typically accomplished by sacrificing carrier transport.

Additionally, a variety of practical applications subject NCs to elevated operating temperatures,[2,3,5,6] and others require processing at elevated temperatures prior to use, both conditions under which significant loss in PL efficiency occurs for reasons that are the focus of current study.[12−20] Volatility or decomposition of organic compounds, and the associated loss of surface passivation, diminishes the utility of organically capped NC cores under these circumstances,[21,22] while core/shell structures appear less susceptible to the effects of elevated temperature.[12]

Small inorganic ligands have recently garnered interest as a new surface passivation option, one that achieves electronic passivation while providing a conductive rather than insulating surface and interstitial medium.[21,23−25] Among inorganic capping ligands, molecular metal chalcogenides

* Address correspondence to schaller@anl.gov, schaller@northwestern.edu.

Received for review November 8, 2013 and accepted December 16, 2013.

Published online December 16, 2013
10.1021/nn405811p

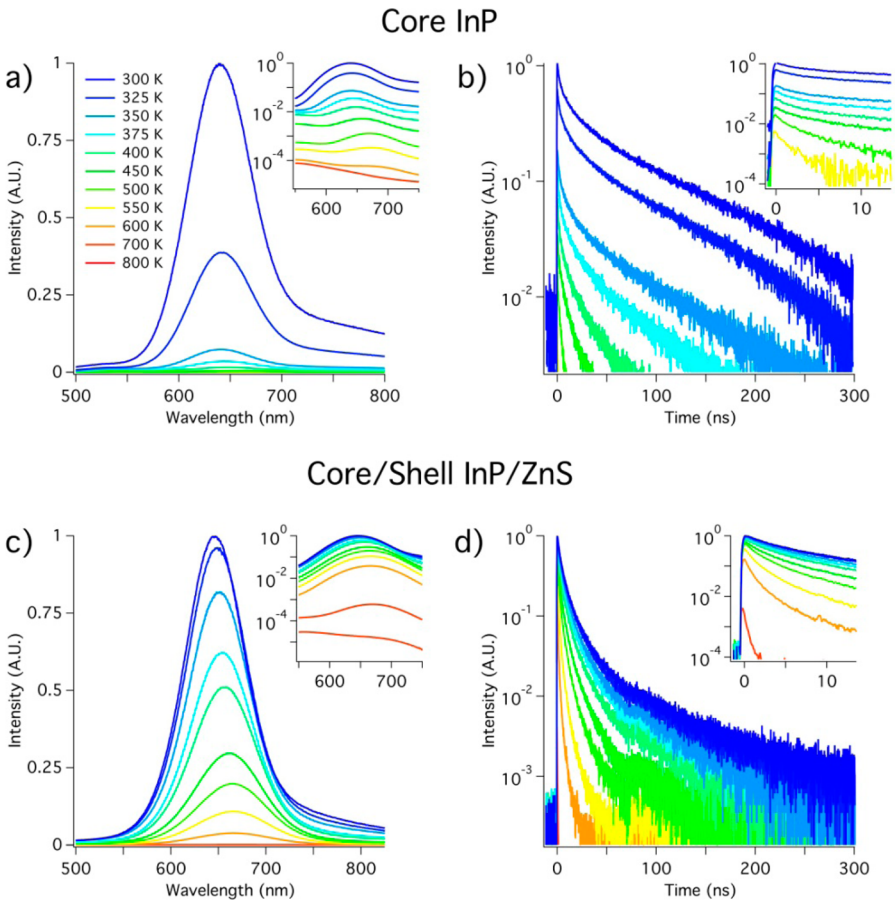

Figure 1. Static and time-resolved PL of InP core NCs (a and b) and InP/ZnS core/shell NCs (c and d) show decreased emission and excited-state lifetimes with increasing temperature.

(MCCs) like $Sn_2S_6^{4-}$, decompose at fairly low temperature to yield a conductive, interstitial "glue" phase that acts as an effective charge transporter.[21] Other inorganic ligands, including chalcogenides, hydrochalcogenides, and hydroxide, are similarly of interest as alternatives to organic capping ligands.[25]

Here, we examine the effects of elevated temperature on the photophysical properties of colloidally synthesized InP NCs. In particular, we track the static and time-resolved PL (trPL) behavior of InP cores and InP/ZnS core/shells of several sizes from 300 to 800 K, where InP cores show significantly greater losses of PL efficiency than do similarly sized InP/ZnS samples. We additionally examine the effects of inorganic capping ligands S^{2-} and $Sn_2S_6^{4-}$ over the same temperature range and find that the addition of these ligands to InP NC cores markedly improves retention of PL properties. We follow the reversibility of PL loss using cyclical heating profiles and find that InP/S^{2-} performs comparably to InP/ZnS. Femtosecond transient absorption (TA) measurements show rapid decay of the lowest-energy bleach feature at elevated temperature, which suggests that loss of PL in InP NCs arises primarily through electron trapping. Finally, we develop a model to better understand the effects of temperature through separating irreversible and total PL loss, calculating the effects of capping ligands on electronic structure, and examining the thermal stability of the surface passivating media. Overall, these findings point to capping with inorganic ligands as an excellent, thermally robust alternative to the use of a ZnS shell, where the latter is undesirable for its physically and electronically insulating properties. This work suggests that inorganic ligands present a promising approach for use in applications that require elevated temperature operation or material processing.

RESULTS AND DISCUSSION

A dramatic decrease in static PL and PL decay times occurs in InP and InP/ZnS samples with temperature elevation, as shown in Figure 1. This decrease is most obvious for InP NC cores, in which more than half the PL intensity is lost upon elevation of the sample temperature to 325 K, and by 350 K, PL intensity has dropped by more than an order of magnitude. In contrast, InP/ZnS core/shell NC samples exhibit nearly unchanged static PL upon elevation to 325 K, and only at 550 K does the static PL finally approach an order of magnitude decrease from ambient temperature. Both samples show a change in trPL associated with

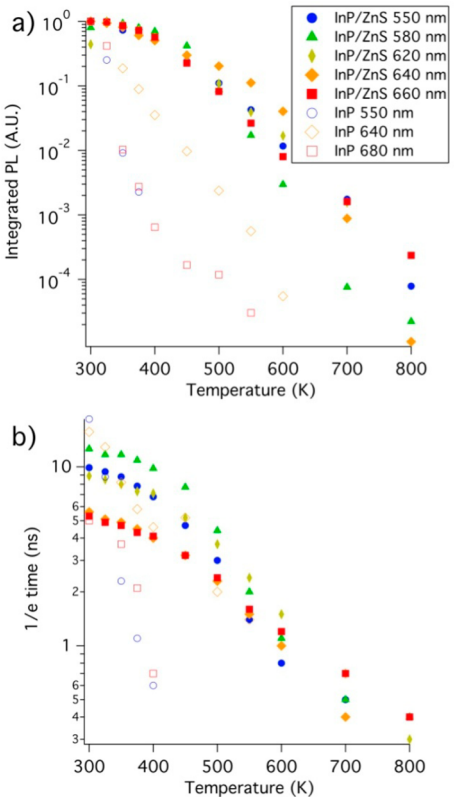

Figure 2. Integrated static PL (a) and trPL (b) for three InP core-only NC samples and five InP/ZnS core/shell samples show a greater temperature effect in core samples with increasing temperature than with core/shell samples. Samples are labeled according to their maximum emission wavelength at room temperature, with 550, 580, 620, 640, 660, and 680 nm sampled corresponding to InP core diameters of 2.9, 3.2, 3.6, 3.9, 4.2, and 4.6 nm, respectively.[26]

decreasing excited-state lifetimes, with the core-only sample exhibiting a more rapid decline in the radiative lifetime than the core/shell sample.

In Figure 2, integrated static PL and excited-state decay times (1/e times) are shown for several InP cores and InP/ZnS core/shell samples. Samples with emission maxima at 550, 580, 620, 640, 660, and 680 nm were measured, corresponding to InP core diameters of 2.9, 3.2, 3.6, 3.9, 4.2, and 4.6 nm, respectively.[26] The core/shell samples show remarkable similarity in their behavior, exhibiting no apparent size-dependence. Integrated PL declines modestly between 300 and 400 K, after which the drop-off is more pronounced. By 800 K, PL intensity has decreased by approximately 4 orders of magnitude. PL decay lifetimes for core/shell samples drop from about 10 ns at 300 K to about 0.5 ns at 700 K. Core samples show greater disparity in their temperature-dependent behavior, but no size-related trend can be extrapolated. All core samples experience a more rapid decline in integrated PL, with significant losses occurring between 300 and 400 K (1−3 orders of magnitude). PL decay lifetimes also decline more rapidly than for core/shell NCs in two out of three core samples. In core-only samples, both static PL and trPL

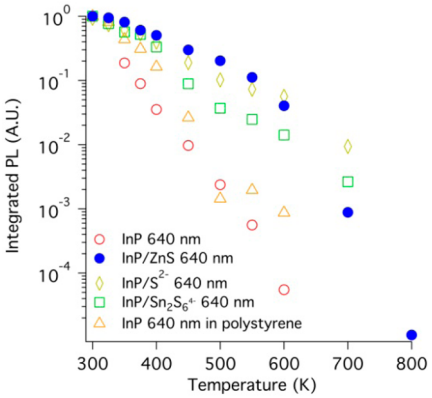

Figure 3. Integrated PL intensity for InP organically capped cores, InP cores in a polystyrene matrix, InP cores capped with inorganic ligands (S^{2-} and $Sn_2S_6^{2-}$), and InP/ZnS core/shell NCs are plotted as a function of sample temperature.

drop to undetectable levels before 800 K. Most notably, this occurs with the smallest InP core by 375 K. Maximum emission wavelength exhibits a gradual redshift with increasing temperature, consistent with the Varshni effect (see Supporting Information, S4).

The instability of organic compounds, which have been shown by thermogravimetric analysis to become volatile around 450 K in CdSe NCs,[22] may lead to an increased number of surface trap states at elevated temperature, which would exacerbate carrier trapping to a greater degree in core-only NCs than in inorganically clad core/shell compositions. If this is indeed the case, the selection of a ligand with greater thermal stability could lead to improved PL robustness at elevated temperatures. To investigate the effects of the ligand on PL, the 630 nm InP core sample was capped with inorganic ligands S^{2-} and $Sn_2S_6^{4-}$. Integrated PL intensity for these NCs is compared with organically capped InP cores, InP cores in a polystyrene matrix, and InP/ZnS core/shell NCs in Figure 3. InP cores with organic capping ligands perform most poorly in terms of exciton stability, experiencing 4 orders of magnitude of PL intensity loss by 600 K before PL becomes undetectable. InP cores embedded in a polystyrene matrix perform only slightly better. By contrast, InP cores capped with S^{2-} and $Sn_2S_6^{4-}$ continue to emit to higher temperature (700 K) and do so at levels similar to InP/ZnS core/shell NCs. Excited-state decay lifetimes of the various samples behave in a similar fashion, with InP cores showing markedly less thermal robustness than inorganically capped NCs. These results are further discussed below (see Quenching Mechanism).

To differentiate between reversible and irreversible effects of elevated temperature on InP, InP/ZnS, and inorganically capped NCs, cyclical heating experiments were performed, in which temperature was ramped up, data were collected, and then temperature was returned to 300 K before repeating the cycle. As shown in Figure 4, InP cores show nearly an order of

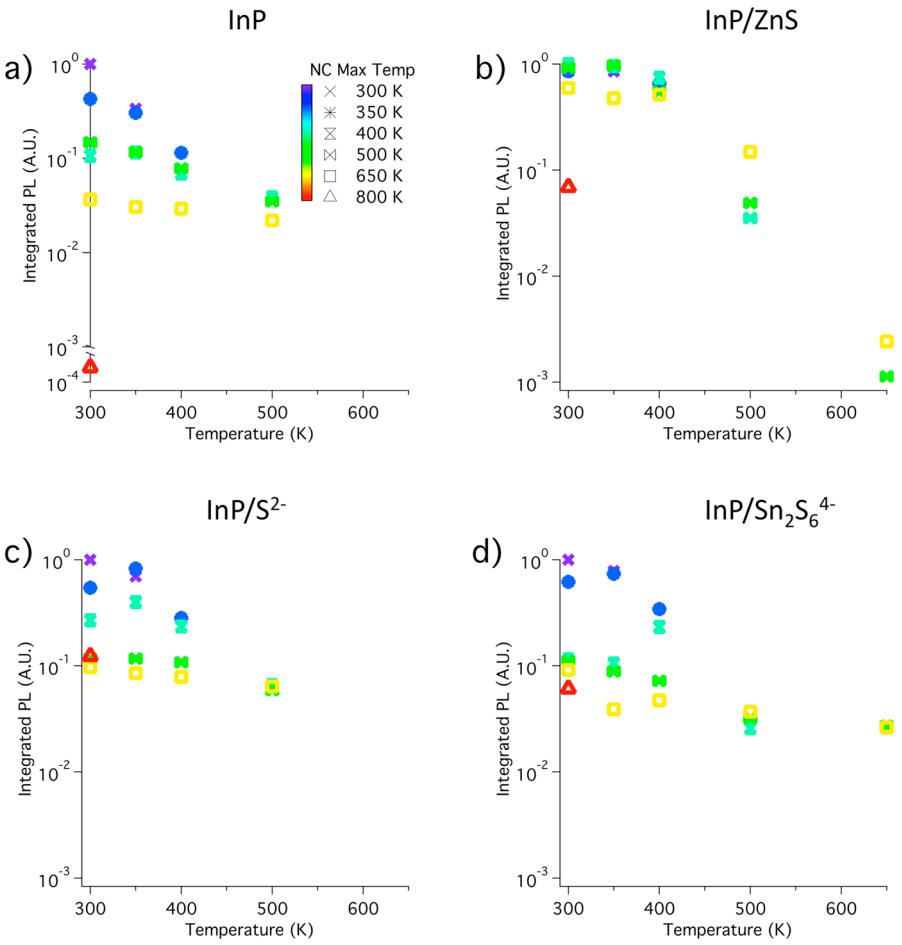

Figure 4. Integrated static PL is shown here for InP, InP/ZnS, InP/S^{2-}, and InP/$Sn_2S_6^{4-}$ subjected to cyclical heating. Data are plotted as a function of the measurement temperature, and symbols and colors correspond to the maximum temperature to which NCs were raised in the previous heating cycle. InP/ZnS and InP/S^{2-} NCs recover more resiliently after heating than do InP and InP/$Sn_2S_6^{4-}$ NCs.

magnitude loss in PL at 300 K after temperature elevation to just 400 K, while InP/ZnS NCs show near complete PL recovery in this same temperature regime. Differences become more dramatic with higher temperature elevation, with InP core-only NCs recovering just 2% of their initial PL intensity after subjection to 650 K, as compared to 60% in InP/ZnS NCs. InP/$Sn_2S_6^{4-}$ and InP/S^{2-} NCs show recovery intermediate between core and core/shell NCs. They do not exhibit the near-total PL recovery that is evident for core/shell NCs in the lower temperature regime (300−400 K), but they do recover more thoroughly and persist to higher temperatures than core-only NCs. In the higher temperature regime (500+ K), inorganically capped samples show PL behavior similar to InP/ZnS, and particularly remarkable is the recovery that both of these inorganically capped samples exhibit after heating to 800 K, which is on par with the InP/ZnS sample. Trends in PL decay lifetimes are weaker, with initial differences among samples exceeding their temperature-induced changes (see Supporting Information, S5).

To compare static PL and PL decay times directly, we employ the relationship between quantum efficiency (QE) and radiative and nonradiative rates, QE = $k_r/(k_{nr} + k_r)$, where QE is proportional to the measured PL intensity. From 1/e times and a measured radiative lifetime of 90 ns (obtained from fitting the long-lived PL feature in the brightest InP core-only sample at 300 K using an exponential decay function), we can thus derive a value based on the 1/e time that is related to PL intensity by a constant. The normalized calculated and experimental PL intensities trend similarly; however, we find that the experimental PL intensities decrease more rapidly than would be predicted based on the 1/e times (see Supporting Information, S6). Some of this discrepancy arises from finite temporal resolution of time correlated single photon counting (TCSPC), which artificially increases reported 1/e times as these values approach the instrument response time. Moreover, energy transfer among NCs within the films likely further exacerbates this discrepancy owing to rapid exciton quenching at some NC energy-acceptor sites despite a lack of carrier trapping at some donor sites.

Quenching Mechanism. Figure 5 shows decay times determined from analysis of both trPL and TA decay

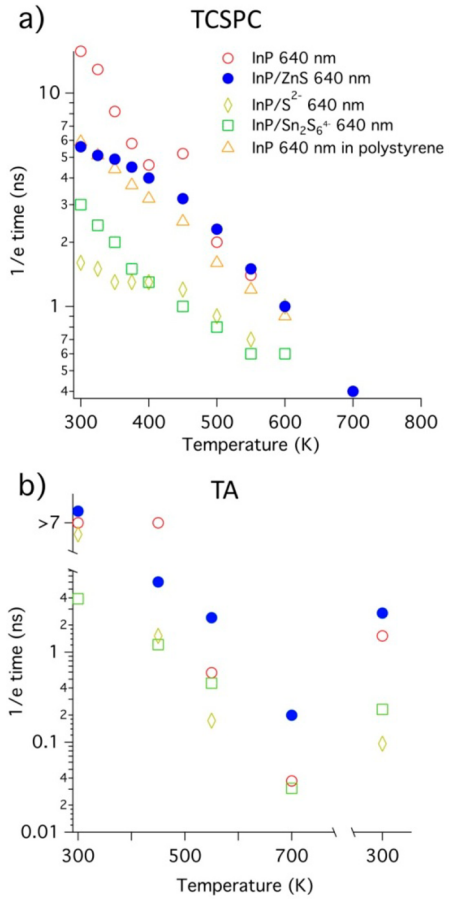

Figure 5. (a) PL decay times (1/e times) derived from TCSPC are plotted against sample temperature. (b) Decay times of bleach maxima from TA (1/e times) are plotted against sample temperature and closely match similar 1/e times from TCSPC.

profiles, where TA dynamics were examined at the wavelength corresponding to the lowest-energy bleach maximum (see also Supporting Information, S7). Here we observe strong correlations between trPL and TA dynamics. Although the former dynamics relay the radiative recombination of electron–hole exciton pairs, quenched PL dynamics cannot help to differentiate among processes that perturb the electron, the hole, or the collective electron–hole pair. TA dynamics examined at the bleach maximum, by contrast, highlight specifically the involvement of the electron. The observed change in TA dynamics with increasing temperature, which conveys electron involvement, eliminates hole trapping as the sole means of PL quenching. Loss of the entire electron–hole pair, through processes such as exciton deactivation could account for the change in TA dynamics, yet a relatively small Huang–Rhys parameter ($S = 0.01$) is indicative of high energetic barriers to phonon-driven relaxation, making exciton deactivation an unlikely route to PL quenching in this material.[27,28] The strong correlation between trPL and TA dynamics shown in Figure 5 indicates that the electron-related process is responsible

TABLE 1. Values of Temperature Sensitivity Parameters ζ_{PL} and ζ_{attr} for InP, InP/ZnS, InP/$Sn_2S_6^{4-}$, and InP/S^{2-}, Where High ζ Values Correspond to Low PL Quenching

	ζ_{PL} (K)	ζ_{attr} (K)
InP core	43(6)	28(2)
InP/ZnS core/shell	137(10)	215(61)
InP/S^{2-}	109(5)	83(10)
InP/$Sn_2S_6^{4-}$	87(6)	28(1)

for the majority of PL quenching, and we thereby conclude that PL quenching does not arise from a combination of electron- and hole- related processes. On the basis of the data, therefore, photoexcited electron trapping is most likely responsible for temperature-driven PL quenching in InP NCs.

Modeling. Several considerations must be explored in order to reach a comprehensive understanding of the differences among the core/shell, organically capped, and inorganically capped InP NCs. Among these are (a) differences between the effects of reversible and irreversible PL loss in isolation, (b) differences in electronic structure between organically and inorganically capped NCs, and (c) the relative thermal stability of the capping ligands.

We use the following general expression to describe PL intensity at a given temperature, T (in Kelvin), in this system:

$$I(T) = I_o - A_{ttr}(T) - R_{ev}(T) \quad (1)$$

That is, the PL intensity as a function of temperature, $I(T)$, is equal to the initial PL intensity (at 300 K), I_o, minus losses from irreversible or attrition processes, $A_{ttr}(T)$, and reversible processes, $R_{ev}(T)$. The reversible processes result in the excited state dynamics that we show above are associated with electron trapping (see Quenching Mechanism). The origin of the irreversible processes will be explored following quantification.

The observed monoexponential decrease of PL intensity with increasing temperature, shown in Figure S8, implies a first-order dependence. Thus, each of the terms in Expression 1 can be expressed in terms of a general differential equation having the form shown below:

$$\frac{dI(T)}{dT} = \frac{-I(T)}{\zeta} \quad (2)$$

Expression 2 relates the change in PL intensity with temperature to ζ, an empirical temperature sensitivity parameter. Solving the differential over the temperature range explored experimentally, we obtain a rate law-like expression for total PL intensity, $I(T) = A\, e^{[-(T-300)/\zeta_{PL}]}$, where $A = 1$ for data normalized to 300 K values. Values of ζ_{PL} from InP, InP/ZnS, InP/$Sn_2S_6^{4-}$, and InP/S^{2-} are summarized in Table 1, where higher values describe less significant PL quenching with temperature elevation.

To isolate NC attrition processes, we re-plot the data from cyclical heating experiments as PL intensity at 300 K *versus* maximum (annealing) temperature, where attrition corresponds to the difference between initial PL intensity and intensity of the annealed sample at 300 K following temperature elevation (see Supporting Information, S8). The resulting curve is fitted with an exponential function, $A_{ttr}(T) = I_0 + A\ e^{[-(T-300)/\zeta_{attr}]}$, in which $I_0 = -A = 1$ when data have been normalized, and ζ_{attr} is an empirical parameter describing the degree of attrition. A high ζ_{attr} corresponds to low levels of attrition and *vice versa*. These values are summarized in Table 1.

Thus over a temperature range beginning at 300 K and for normalized data, Expression 1 can be rewritten as

$$e^{[-(T\ -\ 300)/\zeta_{PL}]} = 1 - e^{[-(T\ -\ 300)/\zeta_{attr}]} - R_{ev}(T) \quad (3)$$

where the term $R_{ev}(T)$ arises from reversible electron trapping that here remains unquantified. InP cores experience the greatest total PL loss, as was obvious in earlier data, but this expression also shows that cores experience the greatest levels of attrition. InP/ZnS core/shell samples are least affected by the heating process, and the inorganically capped samples, with intermediate ζ_{PL} and ζ_{attr} values, fall between the InP and InP/ZnS extremes.

Using density functional theory (DFT), we further examine these structures with the aim of discerning the influence of surface passivation on the overall electronic structure of the NC. Indeed, the lack of size dependence in thermal stability suggests that the surface effects likely dominate PL loss processes. Faceted InP nanocrystals having the zinc blende crystal structure and a 1.6 nm diameter were constructed and passivated with hydrogen and sulfur atoms. Hydrogen passivation was accomplished by placing hydrogen atoms at tetrahedral positions for any In and P atoms having fewer than four bonds. Sulfur passivation was accomplished by placing sulfur atoms in positions corresponding to the lowest energy structure for a S-passivated InP surface.[29] This structure consists of sulfur atoms on the InP surface as well as a layer of sulfur atoms beneath the top layer of In atoms on (001) faces. DFT calculations were carried out using the Vienna Ab-initio Simulation Package (VASP)[30] with supplied Projector Augmented Wave (PAW) potentials for core electrons.[31]

Atomic positions for each structure were relaxed until the forces acting on each atom were less than 0.02 eV/A, after which the electronic density of states (DOS) was calculated for each particle. Figure 6a shows the total and atom-projected DOS for a hydrogen-terminated InP nanocrystal. The total DOS for the sulfur-terminated particle is shown in Figure 6b. In each calculation, the highest occupied molecular orbital (HOMO) has been set to zero energy. Overall, the DOS is qualitatively similar for each structure, with a few exceptions. The valence band maximum for the sulfur terminated particle is dominated by contributions from sulfur atoms, in agreement with previous studies on sulfur-passivated InP (001) surfaces.[29] This contribution may be exaggerated compared to the nanocrystals studied experimentally, which are larger and have a correspondingly decreased surface-to-volume ratio. Two small bands are present at the bottom of the conduction band for the S-passivated nanocrystal (Figure 6b). We find these bands to have trap-like character, rather than being strongly associated with the NC core. Figure 6c shows the charge density associated with these states projected onto the NC electronic structure. Circles and arrows drawn from Figure 6b indicate the origin of each charge density plot in Figure 6c. The two small bands that are clearly below the main conduction band localize charge primarily in sulfur p-type orbitals and on In−S species on the NC surface. By contrast, states wholly within the conduction band exhibit charge density more evenly distributed through the NC, as shown in the bottom structure of Figure 6c. Discounting the trap-like states at the conduction band minimum, we find similar energy gaps for the hydrogen-passivated and sulfur-passivated nanocrystal (1.35 and 1.37 eV, respectively).

These results suggest that the thermal stability imparted by passivation with inorganic ligands is not due to modification of the NC electronic structure. Instead, negligible differences in the electronic structure point to a temperature-driven change in atomistic conditions, the consideration of which merits a closer investigation of the thermal stability of the surface-passivating media. Degradation of the surface passivants would be expected to lead to surface defects and reconstructions, which would provide precisely the carrier trap sites that could account for irreversible PL loss.

A decomposition reaction is known to take place in molecular metal chalcogenides (MCCs) like $Sn_2S_6^{4-}$ around 450 K, wherein $(N_2H_5)_4Sn_2S_6 \rightarrow 2SnS_2 + 4N_2H_4 + 2H_2S$.[21] Thermogravimetric analysis of CdSe NCs capped with $Sn_2S_6^{4-}$, however, shows little loss of mass (3.8%),[23] which occurs gradually between 300 and nearly 600 K. This experiment implies that the main decomposition product remaining, SnS_2, a known participant in charge transport, is relatively nonvolatile. This stability is further supported by TGA of bulk metal−$Sn_2S_6^{4-}$ complexes, in which TGA shows weight loss corresponding to the degradation of a surfactant but not indicative of loss of the MCC at temperatures up to nearly 900 K.[32]

Regarding sulfur-passivated InP, previous studies have demonstrated extremely low volatility of the capping ligand, with samples enduring temperatures as high as 730 K without signs of decomposition.[33] Hence, over the region studied, only at the 800 K data

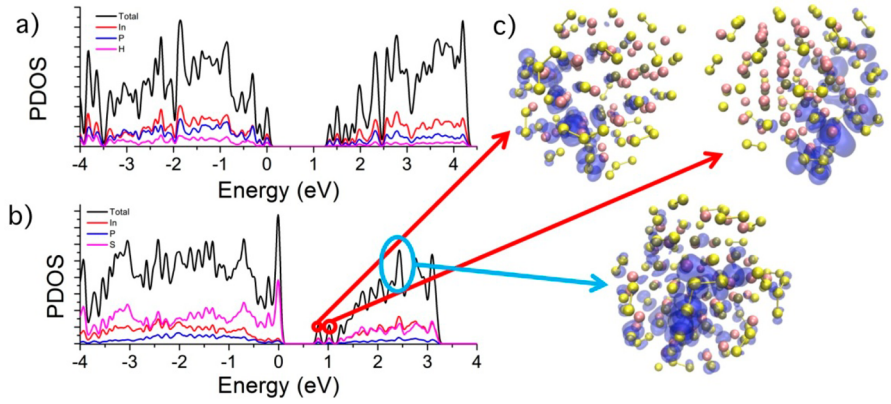

Figure 6. (a) DFT-derived electronic density of states for a hydrogen terminated InP nanocrystal (black curve). The PDOS for each atomic species is also shown: In (red curve), P (blue curve), H(pink curve). (b) DFT-derived electronic density of states for a sulfur terminated InP nanocrystal (black curve). The PDOS for each atomic species is also shown: In (red curve), P (blue curve), S(pink curve). (c) Lowest energy structure for a sulfur-terminated InP nanocrystal with three different charge densities, each associated with a region of the DOS indicated in (b). The red arrows indicate the trap-like states at the conduction band edge, while the blue arrow indicates a "core-like" state with charge density through the nanocrystal structure.

point—at which InP/S^{2-} PL is no longer detectable—do we anticipate ligand volatility to play a role in PL suppression. This stability is in keeping with the low vapor pressure of similar compounds (*e.g.*, GaS) in this temperature regime.[34]

By contrast, organic capping ligands show significantly greater volatility, and their departure likely terminates their role in passivating the surface of the NC.[35,36] Indeed, thermogravimetric analysis of TOPO, the ligand used to passivate the InP core surface, shows near-complete weight loss between 460 and 580 K (Supporting Information, S9). Thus, at temperatures as low as 500 K, organic ligands are expected to volatilize and likely leave behind surface trap states available to carriers, resulting in irreversible PL quenching. In this regime, however, sulfide and MCCs are expected to remain stable and to continue to play a role in surface passivation and, further, in charge transport.

CONCLUSIONS

InP NCs exhibit a loss of static and time-resolved PL with increasing temperature in which the method of surface passivation plays a significant role. Organically capped NCs suffer from irreversible and reversible PL loss to a much greater degree than do InP/ZnS, InP/$Sn_2S_6^{4-}$, and InP/S^{2-} NCs. Among the latter, InP/S^{2-} NCs recover particularly well in cyclical heating experiments. These properties are especially important in device manufacturing with high-temperature processing steps as well as in applications that subject NCs to elevated temperature operating conditions (*e.g.*, LEDs, lasers, *etc.*).

Coupled with trPL data, TA measurements point to electron-related processes as the primary quenching mechanism in InP materials; and the relatively high energetic barrier to phonon-driven relaxation points to electron trapping (rather than exciton deactivation) as the dominant quenching mechanism. Using a quantitative model, we divorce attrition of NCs from total PL loss, and DFT calculations show relatively similar electronic structure among sulfide and organically capped NCs. Combined with a knowledge of the thermal stability of the surface passivation media and a lack of size-dependence in experimental PL quenching data, we conclude that thermal stability is related to surface rather than core processes.

METHODS

InP NCs with a lowest-energy excitonic peak redder than 580 nm were synthesized following a known procedure from $InCl_3$ and tris(trimethylsilyl)phosphine, $(TMS)_3P$, using a 10:1 (by weight) mixture of trioctylphosphine (TOP) and trioctylphosphine oxide (TOPO) and annealing at 270 °C for 24 h.[37] Size selective precipitation was performed to obtain a series of monodisperse InP NCs. InP samples with the first excitonic peak to the blue of 580 nm were synthesized from $In(ac)_3$ and myristic acid in octadecene, to which were added $(TMS)_3P$ and 1-octylamine in octadecene.[38] To synthesize inorganically capped InP NCs, a ligand exchange process, in which organic surfactants were displaced by S^{2-} or $Sn_2S_6^{4-}$ inorganic ligands, was carried out on one of the InP samples.[24,25] For complete synthetic details, refer to Supporting Information, S1–3. InP/ZnS core/shell NCs capped with oleylamine were obtained commercially from NN-Labs. Studied InP samples exhibited high PL quantum yields in the range of 15–35%. All samples are labeled in figures according to the maximum emission peak observed at ambient temperature.

NCs were drop cast from toluene onto glass slides and mounted in an evacuated optical oven. For time-integrated PL and trPL derived from TCSPC, samples were photoexcited using a 45-ps pulsewidth, 405 nm diode laser operated between 2.5 and 40 MHz. PL was collected with a quartz lens and coupled into a fiber optic that routed photons to a 300 mm grating spectrograph. Static PL spectra were collected using a thermoelectrically cooled CCD. Integrated PL intensity was determined by fitting static PL spectra with a Gaussian function and integrating the area, a routine that was particularly important for spectra where trap emission overlapped with the band-edge

emission signal. TCSPC was recorded using an avalanche photodiode at the temperature-dependent PL spectrum maximum.

TA measurements were performed using a 35-fs amplified titanium:sapphire laser operating at 2 kHz. A portion of the laser output at 1.55 eV was mechanically time-delayed and focused into a sapphire plate to produce a white light. Pump pulses at 3.1 eV were mechanically chopped to 1 kHz, overlapped with the probe pulse on the sample, and adjusted to an intensity corresponding to less than 1 exciton per NC on average.

In one-way heating experiments, the oven temperature was increased incrementally from 300 to 800 K. At each temperature, the sample was equilibrated for 10 min before optical data were collected. In cyclical heating experiments, the temperature was similarly ramped and permitted to equilibrate; however, here the temperature was returned to 300 K each time a new high temperature was reached.

Conflict of Interest: The authors declare no competing financial interest.

Supporting Information Available: Synthetic details, emission wavelengths as a function of sample temperature, PL decay times for temperature cycling experiments, kinetic traces from TA data, fits for PL loss, and TGA of TOPO. This material is available free of charge *via* the Internet at http://pubs.acs.org.

Acknowledgment. Use of the Center for Nanoscale Materials was supported by the U.S. Department of Energy, Office of Science, Office of Basic Energy Sciences, under Contract No. DE-AC02-06CH11357. C.E.R and D.C.H acknowledge support by a National Science Foundation Graduate Research Fellowship under Grant No. DGE-0824162.

REFERENCES AND NOTES

1. Anikeeva, P. O.; Halpert, J. E.; Bawendi, M. G.; Bulović, V. Electroluminescence from a Mixed Red−Green−Blue Colloidal Quantum Dot Monolayer. *Nano Lett.* **2007**, *7*, 2196–2200.
2. Buso, S.; Spiazzi, G.; Meneghini, M.; Meneghesso, G. Performance Degradation of High-Brightness Light Emitting Diodes Under DC and Pulsed Bias. *IEEE Trans. Device Mater. Reliab.* **2008**, *8*, 312–322.
3. Bachmann, V.; Ronda, C.; Meijerink, A. Temperature Quenching of Yellow Ce^{3+} Luminescence in YAG:Ce. *Chem. Mater.* **2009**, *21*, 2077–2084.
4. Klimov, V. I.; Mikhailovsky, A. A.; Xu, S.; Malko, A.; Hollingsworth, J. A.; Leatherdale, C. A.; Eisler, H.-J.; Bawendi, M. G. Optical Gain and Stimulated Emission in Nanocrystal Quantum Dots. *Science* **2000**, *290*, 314–317.
5. Braithwaite, J.; Silver, M.; Wilkinson, V. A.; O'Reilly, E. P.; Adams, A. R. Role of Radiative and Nonradiative Processes on the Temperature Sensitivity of Strained and Unstrained 1.5 μm InGaAs(P) Quantum Well Lasers. *Appl. Phys. Lett.* **1995**, *67*, 3546–3548.
6. Royne, A.; Dey, C. J.; Mills, D. R. Cooling of Photovoltaic Cells under Concentrated Illumination: A Critical Review. *Sol. Energy Mater. Sol. Cells* **2005**, *86*, 451–483.
7. Pattantyus-Abraham, A. G.; Kramer, I. J.; Barkhouse, A. R.; Wang, X.; Konstantatos, G.; Debnath, R.; Levina, L.; Raabe, I.; Nazeeruddin, M. K.; Grätzel, M.; *et al.* Depleted-Heterojunction Colloidal Quantum Dot Solar Cells. *ACS Nano* **2010**, *4*, 3374–3380.
8. Alivisatos, A. P.; Gu, W.; Larabell, C. Quantum Dots As Cellular Probes. *Annu. Rev. Biomed. Eng.* **2005**, *7*, 55–76.
9. Talapin, D. V.; Murray, C. B. PbSe Nanocrystal Solids for n- and p-Channel Thin Film Field-Effect Transistors. *Science* **2005**, *310*, 86–89.
10. Snee, P. T.; Somers, R. C.; Nair, G.; Zimmer, J. P.; Bawendi, M. G.; Nocera, D. G. A Ratiometric CdSe/ZnS Nanocrystal pH Sensor. *J. Am. Chem. Soc.* **2006**, *128*, 13320–13321.
11. Somers, R. C.; Bawendi, M. G.; Nocera, D. G. CdSe Nanocrystal Based Chem-/Bio-Sensors. *Chem. Soc. Rev.* **2007**, *36*, 579–591.
12. Rowland, C. E.; Schaller, R. D. Exciton Fate in Semiconductor Nanomaterials at Elevated Temperatures: Hole Trapping Out-Competes Exciton Deactivation. *J. Phys. Chem. C* **2013**, *117*, 17337–17343.
13. Cai, X.; Martin, J. E.; Shea-Rohwer, L. E.; Gong, K.; Kelley, D. F. Thermal Quenching Mechanisms in II−VI Semiconductor Nanocrystals. *J. Phys. Chem. C* **2013**, *117*, 7902–7913.
14. Valerini, D.; Cretí, A.; Lomascolo, M.; Manna, L.; Cingolani, R.; Anni, M. Temperature Dependence of the Photoluminescence Properties of Colloidal CdSe/ZnS Core/Shell Quantum Dots Embedded in a Polystyrene Matrix. *Phys. Rev. B* **2005**, *71*, 235409.
15. Zhao, Y.; Riemersma, C.; Pietra, F.; Koole, R.; de Mello Donegá, C.; Meijerink, A. High-Temperature Luminescence Quenching of Colloidal Quantum Dots. *ACS Nano* **2012**, *6*, 9058–9067.
16. Narayanaswamy, A.; Feiner, L. F.; van der Zaag, P. J. Temperature Dependence of the Photoluminescence of InP/ZnS Quantum Dots. *J. Phys. Chem. C* **2008**, *112*, 6775–6780.
17. Narayanaswamy, A.; Feiner, L. F.; Meijerink, A.; van der Zaag, P. J. The Effect of Temperature and Dot Size on the Spectral Properties of Colloidal InP/ZnS Core−Shell Quantum Dots. *ACS Nano* **2009**, *3*, 2539–2546.
18. Biju, V.; Makita, Y.; Sonoda, A.; Yokoyama, H.; Baba, Y.; Ishikawa, M. Temperature-Sensitive Photoluminescence of CdSe Quantum Dot Clusters. *J. Phys. Chem. B* **2005**, *109*, 13899–13905.
19. Yu, H. C. Y.; Leon-Saval, S. G.; Argyros, A.; Barton, G. W. Temperature Effects on Emission of Quantum Dots Embedded in Polymethylmethacrylate. *Appl. Opt.* **2010**, *49*, 2749–2752.
20. Pugh-Thomas, D.; Walsh, B. M.; Gupta, M. C. CdSe(ZnS) Nanocomposite Luminescent High Temperature Sensor. *Nanotechnology* **2011**, *22*, 185503.
21. Talapin, D. V.; Lee, J.-S.; Kovalenko, M. V.; Shevchenko, E. V. Prospects of Colloidal Nanocrystals for Electronic and Optoelectronic Applications. *Chem. Rev.* **2010**, *110*, 389.
22. Porter, V. J.; Geyer, S.; Halpert, J. E.; Kastner, M. A.; Bawendi, M. G. Photoconduction in Annealed and Chemically Treated CdSe/ZnS Inorganic Nanocrystal Films. *J. Phys. Chem. C* **2008**, *112*, 2308–2316.
23. Kovalenko, M. V.; Scheele, M.; Talapin, D. V. Colloidal Nanocrystals with Molecular Metal Chalcogenide Surface Ligands. *Science* **2009**, *324*, 1417–1420.
24. Liu, W.; Lee, J.-S.; Talapin, D. V. III-V Nanocrystals Capped with Molecular Metal Chalcogenide Ligands: High Electron Mobility and Ambipolar Photoresponse. *J. Am. Chem. Soc.* **2013**, *135*, 1349–1357.
25. Nag, A.; Kovalenko, M. V.; Lee, J.-S.; Liu, W.; Spokoyny, B.; Talapin, D. V. Metal-free Inorganic Ligands for Colloidal Nanocrystals: S^{2-}, HS^{-}, Se^{2-}, HSe^{-}, Te^{2-}, HTe^{-}, TeS^{3-}, OH^{-}, and NH^{2-} as Surface Ligands. *J. Am. Chem. Soc.* **2011**, *133*, 10612–10620.
26. Mićić, O. I.; Cheong, H. M.; Fu, H.; Zunger, A.; Sprague, J. R.; Mascarenhas, A.; Nozik, A. J. Size-Dependent Spectroscopy of InP Quantum Dots. *J. Phys. Chem. B* **1997**, *101*, 4904–4912.
27. Hamma, M.; Miranda, R. P.; Vasilevskiy, M. I.; Zorkani, I. Calculation of the Huang−Rhys Parameter in Spherical Quantum Dots: The Optical Deformation Potential Effect. *J. Phys.: Condens. Matter* **2007**, *19*, 346215.
28. Ridley, B. K. *Quantum Processes in Semiconductors*; Oxford University Press: Oxford, 1999.
29. Li, D.-F.; Xiao, H.-Y.; Xue, S.-W.; Yang, L.; Zu, X.-T. Surface Structure and Electronic Property of InP(001)-(2 × 1)S Surface: A First-Principles Study. *Chin. Phys. Lett.* **2010**, *27*, 046802.
30. Kresse, G.; Furthmüller, J. Efficient Iterative Schemes for *ab Initio* Total-Energy Calculations Using a Plane-Wave Basis Set. *Phys. Rev. B* **1996**, *54*, 11169–11186.
31. Kresse, G.; Joubert, D. From Ultrasoft Pseudopotentials to the Projector Augmented-Wave Method. *Phys. Rev. B* **1999**, *59*, 1758–1775.
32. Rangan, K. K.; Trikalitis, P. N.; Canlas, C.; Bakas, T.; Weliky, D. P.; Kanatzidis, M. G. Hexagonal Pore Organization in Mesostructured Metal Tin Sulfides Built with $[Sn_2S_6]^{4-}$ Cluster. *Nano Lett.* **2002**, *2*, 513–517.

33. Anderson, G. W.; Hanf, M. C.; Norton, P. R.; Lu, Z. H.; Graham, M. J. Thermal Stability of Sulfur Passivated InP(100)-(1 × 1). *Appl. Phys. Lett.* **1994**, *65*, 171–173.
34. Lieth, R. M. A.; Heijligers, H. J. M.; v.d. Heijden, C. W. M. The Vapour Pressure and Thermal Stability of Gallium Sulphide. *Mater. Sci. Eng.* **1967**, *2*, 193–200.
35. Foos, E. E.; Wilkinson, J.; Mäkinen, A. J.; Watkins, N. J.; Kafafi, Z. H.; Long, J. P. Synthesis and Surface Composition Study of CdSe Nanoclusters Prepared Using Solvent Systems Containing Primary, Secondary, and Tertiary Amines. *Chem. Mater.* **2006**, *18*, 2886–2894.
36. Ma, J. Preparation and Characterization of ZrO2 Nanoparticles Capped by Trioctylphosphine Oxide (TOPO). *J. Wuhan Univ. Technol., Mater. Sci. Ed.* **2011**, *26*, 611–614.
37. Mićić, O. I.; Curtis, C. J.; Jones, K. M.; Sprague, J. R.; Nozik, A. J. Synthesis and Characterization of InP Quantum Dots. *J. Phys. Chem.* **1994**, *98*, 4966–4969.
38. Xie, R.; Battaglia, D.; Peng, X. Colloidal InP Nanocrystals as Efficient Emitters Covering Blue to Near-Infrared. *J. Am. Chem. Soc.* **2007**, *129*, 15432–15433.